Available online at http://www.sdcjter.in/

SDC Journal of Theoretical and Experimental Research (SDCJTER) 01(01), 2023, 07–15

Structural and Electrical Characterization of Cobalt Oxide Nanoparticles

Srijith S [a*], Asitha L. R [a], Amritha R S [a] and Ridhun M [a]

[a] *Department of Physics, Sree Narayana College, Kollam, India – 691001*

Available online 01January 2023

Abstract

Cobalt oxide (Co_3O_4) is a transition metal oxide. These nanoparticles of Co_3O_4 possess interesting magnetic, optical, field emission as well as electrochemical properties. Thus, they have significant applications in devices like solid-state sensors, solar selective absorbers, lithium batteries, catalysis etc. Thus, it is an industrially significant oxide. Considering the unique potentialities as well as the simplicity of SCS, it is a best option for the synthesis of metal oxide nanomaterials. Average crystallite size was determined using X-ray diffraction line broadening. Nanocrystalline cubic and anisotropic Co_3O_4 sample with an average crystallite size of 11 nm was synthesised. Variation of dc electrical conductivity with temperature was tabulated. From the Arrhenius plot of Co_3O_4, activation energy was evaluated to be 0.51 eV. Co_3O_4 nanoparticles have greater significance in solid state sensors, solar collectors, electrochromic devices and so on.

Keywords: Nanocrystalline; Solution combustion; line broadening; activation energy

1. Introduction

Pure cobalt being not so stable at room temperature, it can get converted to oxides like CoO, Co_2O_3, and Co_3O_4; where Co_3O_4 is the most stable phase. Cobalt oxide with valence greater than 3 is unstable in the natural environment [1]. Both CoO and Co_3O_4 have industrial applications. Co_3O_4 is an intrinsic P-type semiconductor and exhibits normal cubic spinel crystal structure of the form AB_2O_4. The tetrahedral A sites are occupied by the spin moments of $Co^{2+}$and octahedral B sites by the spin moments of Co^{3+} ions. Thus, it can be represented as $Co^{2+}(Co^{3+})_2O_4^{2-}$. Bulk Co_3O_4 possess a lattice constant of 8.08 A^0 . It exhibits antiferromagnetic nature with each Co^{2+}ion in A site have four neighbouring Co^{2+} ions of opposite spin.

* Corresponding author: *Email address*: *srijithkeanu@gmail.com* (Srijith S)

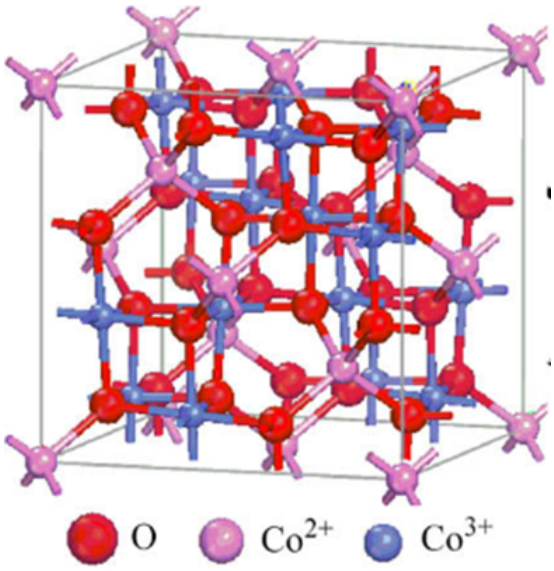

Fig 1 Structure of bulk Co_3O_4

Co_3O_4 nanoparticles possess interesting magnetic, optical, field emission as well as electrochemical properties ascribed by quantum confinement effects. From the IR absorption band studies, it was found that tetrahedrally coordinated M-O has stretching vibration mode and octahedrally coordinated M-O is bound. Band gaps showing blue shift of absorption peaks (low wavelength) specify the semiconducting nature [2]. Hysteresis loop of Co_3O_4 nanoparticles (NP) shows ferromagnetic behaviour. Co_3O_4 NPs are made of small crystalline domains, each having its own magnetic moment oriented randomly. Thus the total magnetic moment equals the sum of these magnetic domains coupled by dipolar interactions. Tricobalt tetroxides own good gas sensing capabilities, this makes them useful in gas sensors. Gas sensors require porous polycrystalline resistors made of semiconducting oxides. Gas sensors, in particular Cobalt monoxide sensing devices make use of Co_3O_4 in detecting the presence of the air pollutant, CO. They are also sensitive to isobutene, CH_4, H_2, NH_3, CO and NO_2 gases at low temperature [2-5]. Cobalt oxide shows good thermal stability at higher temperatures (>500^0c), thus they are functional in solar selective surfaces. Thus for high temperature solar electric absorber Co_3O_4 NPs are used [6]. Use of Co_3O_4 nano powders in selective surfaces of solar collectors helps to improve its energy efficiency. The optical properties of nano Co_3O_4 has significance in applications like solar cells, gas sensors and electrochromic devices [5]. Nano Co_3O_4 has good catalytic property because of increased surface atoms at nano size. They are used as photocatalysts. Co_3O_4 shows high-catalytic activity for the oxidation of CO, N_2O etc. Cobalt oxide (Co_3O_4) powder being magnetic, electrochromic, gas sensing, energy storable as well as highly catalytic material have wide range of realistic applications. This chapter briefly describes the procedure for determining the average crystallite size from X-ray diffraction pattern. Scherrer equation is the simplest method of obtaining crystallite size from X-ray diffraction line broadening. Full Width at Half Maximum is the most convenient

measure of the X-ray diffraction line broadening. As Cobalt oxide (Co3O4) has wide spread use in fields such as electrochemical capacitors, cathode material, etc. measurement of its electrical conductivity is significant. Further description on the experimental setup used for measuring the dc conductivity of the sample is also provided. Usually Co3O4 has a dc electrical resistivity which is semiconducting nature.

2. Experimental set up

Solution Combustion synthesis is a particular type of self-propagating high- temperature synthesis (SCS). [7-9] Combustion is the main source of heat for this self-sustained thermal process. This complex process occurs in a homogenous solution of precursors. A violent self-sustained reaction occurs between an oxidizer and fuel. Citric acid is used as fuel. Here fuel is not only a mere reducer, instead it also plays the role of complexing agent as well as a microstructural template. Fuels preserve the compositional homogeneity between all constituents by preventing the precipitation of metal ions. It acts as a chelating agent. High solubility in the solvent, low decomposition temperature and absence of residual mass after combustion makes a fuel ideal. The fuel taken for the combustion synthesis has to be compatible with the metal nitrates used. By the burning of organic fuel, heat required for combustion is evolved. Finally, solid product is formed with the evolution of significant amount of gases. Solution combustion method of synthesis is a time and energy efficient process capable of producing metal oxide nanomaterials with well-developed porosity. In simple words, SCS is a self-sustained redox reaction initiated by a source of energy, between a fuel and an oxidant (usually metal nitrates). Main constituents of SCS includes oxidizer, reducing agent or fuel and a suitable solvent.

A mixture of high purity Co $(NO_3)_2.6H_2O$ (5 gm) and citric acid (1.59 gm) were properly dissolved in distilled water. All the chemicals used were of analytical grade. After adding nitric acid (20 ml) the solution was heated and stirred magnetically for 30 minutes to make it a homogenous as well as concentrated solution. In order to make the pH value of the solution as 7, adequate amount of ammonium hydroxide (NH_4OH) was added drop by drop into the solution. Again, the mixture was heated until maximum water content in the solution gets evaporated and evolve into a thick gel like solution. The solution thus synthesised was subjected to combustion using an electric coil heater. Mixture frothed and foamed under self-propagating mode of combustion. The resultant powder was calcined in a preheated furnace at 700^0C for 5 hours to remove carbonaceous impurities formed while combustion.

3. RESULTS AND DISCUSSION

3.1 X-ray Diffraction Pattern and Phase Identification of the sample

The crystalline phases and micro strain variation of the samples were identified by X-ray powder diffraction method (XRD) [10]. X-ray diffraction pattern of the nanocrystalline samples were recorded using a **XPERT-PRO** power diffractometer using copper K_α (λ=1.54060 Å) radiation. The sample was scanned over the range 2θ from 10^o to 80^o, with step size of 0.05^o. The X-ray diffraction patterns are shown in Fig 2.

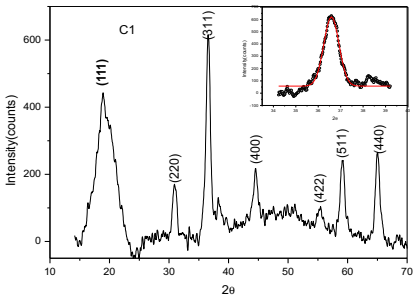

Fig 2 X-ray diffraction pattern of Co_3O_4 sample

The well-defined X-ray diffraction peak confirms the crystalline nature of the sample. Broadened diffraction peak is an indication of small crystallite size. In order to confirm the phase purity of the sample prepared, the inter-planar spacing($\mathbf{d}_{hkl}$) values and relative intensity values ($\mathbf{I/I_o}$) corresponding to the observed diffraction peak of the sample is compared with the standard values of various cobalt oxide samples, viz., CoO, Co_2O_3, Co_3O_4, etc., as reported by JCPDS-International Centre for Diffraction Data. Now, from the Bragg's equation $\mathbf{n\,\lambda = 2d_{hkl}Sin\theta_{hkl}}$, the d_{hkl} value was calculated corresponding to each 2θ values. The $\mathbf{d}_{hkl}$ values and relative intensity values (I/I_0) of diffraction peaks for the sample was compared with **JCPDS-ICDD (**Pattern number-76-1802) for cubic Co_3O_4. It is clear that the sample obtained is Co_3O_4 with cubic symmetry. The small deviation in $\mathbf{d}_{hkl}$ values and relative intensity ($\mathbf{I/I_o}$) values of the sample prepared from the standard value is the general feature of the nanocrystalline materials. It is due to the varied atomic arrangement at the interfaces and the strain due to the large surface area to volume ratio. Another possible reason is the breakdown of long-range order in nanocrystalline samples. X- ray diffraction pattern of the prepared Co_3O_4 sample is shown in the figure 2.

3.2 Determination of Average Crystallite Size Using Scherrer equation

The crystallite sizes of the sample is determined from X-ray diffraction line broadening of the maximum intensity peak corresponding to the (311) reflection using Scherrer equation (11-13). Scherrer equation is used for determining the average crystallite size of a nanocrystalline sample from X-ray diffraction line broadening;

$$\mathbf{t = K\,\lambda / (\beta_{hkl})_{measured} * Cos\Theta_{hkl}} \quad \text{.....(1)}$$

Where **t** - the average crystallite size normal to the reflecting planes, **K** - the shape factor which lies between 0.95 and 1.15 (**K**=1 for spherical crystallites), **λ**-the wavelength of X-rays used, $\mathbf{(\beta_{hkl})_{measured}}$ - Measured FWHM of the diffraction line in radians, θ_{hkl} - The Bragg angle corresponding to the diffraction line arising from reflections from the planes designated by the Miller indices (**h k l**). The FWHM was estimated using the following procedure. A Pseudo-Voigt 1 function which assume the peak shape is symmetrical was used to fit the peak profiles. Pseudo-Voigt 1 is one of the most convenient functions used for the profile fitting of X-ray diffraction peaks and it is represented by the expression,

$$y = y_0 + A\left[\frac{2\omega}{\pi\left(x - x_c\right)^2 + \omega^2} + \frac{(1-\mu)\sqrt{4\ln 2}\left(e^{-\frac{4\ln 2(x-x_c)^2}{\omega}}\right)}{\sqrt{\pi}\omega}\right] \quad \ldots\ldots\ldots\ldots(2)$$

where, y is the dependent variable (Intensity in the present case), X is the dependent variable (2θ in the present case), ie, $\mathbf{X_c}$ is the peak centre, **A** is the measure of maximum intensity and **W** is the Full Width at Half Maximum and **μ** is the profile shape factor. The curve fitting was done using **Microcal Origin Version 6.1.** The best fit was chosen taking into account the minimum error as well as the realistic values for individual variables. In the following procedure, the error occurred on calculating the value of $\boldsymbol{\beta}_{hkl}$ is not included in the calculation for convenience. Thus, the average crystallite size of the sample was calculated from (311) peak of XRD as seen in the table 1.

hkl	**2 θ**	**Θ**	$\boldsymbol{\beta}_{hkl}$	**Crystallite size t (nm)**
111	19	9.5	0.76	11.78
220	31.33	15.655	0.8	11.46
311	36.84	18.42	0.85	10.95
400	44.79	22.395	0.84	11.37
422	55.72	27.86	0.84	11.89
511	59.29	29.645	0.87	11.68
440	65.29	32.645	1	10.49

Table 1 Average crystallite size determination of sample using Scherrer equation

3.3 Hall-Williamson Method to Separate Crystallite Size and Strain Broadening

In this section, Hall-Williamson analyses of the nanocrystalline sample was carried out assuming Uniform deformation model (UDM) (14-16). This model doesn't take into account the anisotropic nature of the crystal. In this model, micro strain **ε** is assumed to be uniform in all crystallographic directions and Hall- Williamson equation can be written as

$$\boldsymbol{\beta}_{hkl}\cos\theta_{hkl} = (K\lambda/t) + (4\langle\boldsymbol{\varepsilon}\rangle\sin\theta_{hkl} \quad (3)$$

Plotting the measured values of $(\beta_{hkl})_{corrected}$ as a function of $(4 \sin\theta_{hkl})$, the micro strain $\langle\varepsilon\rangle$ can be estimated from the slope of the line and the intersection of the vertical axis gives crystallite size. The Hall-Williamson plot assuming uniform deformation model for the sample is shown in Figure 3. In the case of the present sample, the Y-intercept is positive indicating the lattice expansion.

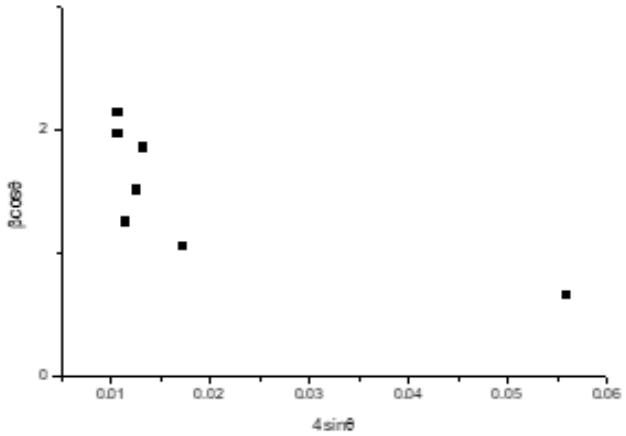

Fig 3 Hall-Williamson plot assuming uniform deformation model.

From the graph, it was noted that the sample plot does not give a linear behaviour. This leads to the inference that, uniform deformation model, which does not take into account of the anisotropic nature of the elastic constants in a crystal is not suitable for analyzing the strain contributions in the case of the present sample. Because its crystal lattice contains defect points or impurity atoms and hence degree of anisotropy increases. Defects can be cation or anion vacancies. Hence strain analysis of the sample can be achieved by some other technique such as Warren-Averbach model.

3.4 Measurement and Analysis of DC Electrical Conductivity

For measuring the dc conductivity of nanocrystalline Co_3O_4 sample, the as prepared sample has to be consolidated into either pellets or as a thick film. If the nano powder could be consolidated into cylindrical pellets, the dc conductivity studies can be done by coating conducting silver or gold electrodes on the two opposite circular surfaces. A suitable dc voltage can be applied across the opposite faces and the current which passes through the pellet can be measured and hence resistance can be estimated. Knowing the thickness and diameter of the pellet, the dc conductivity value can be estimated using Ohm's law, Resistance, $\mathbf{R = (1/\sigma)\ (t/A)}$ where, $\boldsymbol{\sigma}$ is the dc conductivity of the sample, **t** is the thickness and **A** is the area of the cylindrical pellet. The sample was pelletized using a KBr press and a cylindrical die of diameter 13 mm. The pressure applied was 4 tons. Conducting silver epoxy was carefully applied to the opposite circular faces of the pellet to ensure good electrical contact. Then the pellet was spring loaded into a dielectric cell with provision for evacuation and controlling temperature in the range 72 K to 555 K. The dc electrical resistance was measured using a Kiethley 2400 source meter. Here, the measurements were done in a vacuum of about 0.22 millibar and in the temperature range 303 K to 423 K.

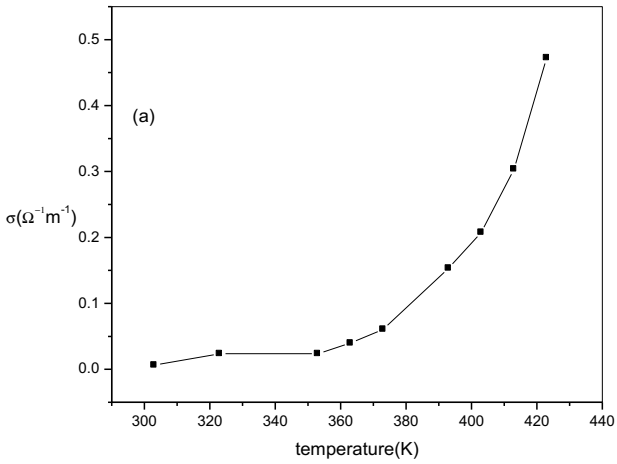

Fig 4 Plot of variations of dc conductivity σ_{dc} with respect to temperature

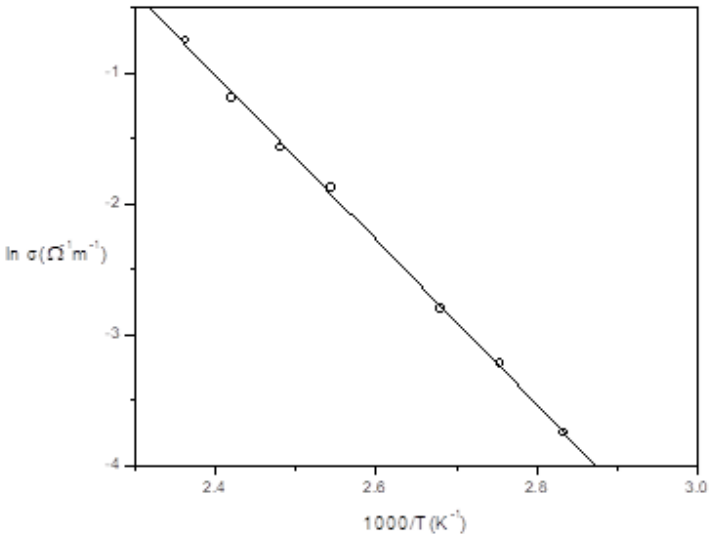

Fig 5 Arrhenius plot of Co_3O_4

In order to estimate the activation energy, Arrhenius plot was plotted as shown in figure 4. For a thermally activated mechanism with exponential dependence, i.e. $\sigma_{dc} = \sigma_0 \exp(-E_a/kT)$, where E_a is the activation energy for conduction, **k** is the Boltzmann's constant, **T** the absolute temperature and σ_0 is a constant. The activation energy for the process can be estimated from the slope of the Arrhenius plot. The activation energies for sample was estimated to be equal to 0.51 eV (17-19). In the case of transition metal oxides, an enhancement in conductivity with decrease in crystallite size is reported. This is interpreted as due to the contribution of large percentage of defects associated with the large percentage of grain boundaries. In the case of nanocrystalline Co_3O_4 samples in the present study, the increase in conductivity is probably due to a decrease in crystallite size. In Co_3O_4, co-exist in two oxidation states +2 and +3. In the temperature range studied, the major conductivity mechanism is the charge transfer between Co^{2+} and Co^{3+} sites (d-d transitions) with an activation energy lying between 0.5 eV and 0.8 eV. The activation energy of 0.51 eV obtained for this sample is in agreement with this inference.

3.5 Conclusion

Nanocrystalline Co_3O_4 was synthesised using solution combustion method with an average crystallite size around 11 nm. From X-ray diffraction, presence of cubic Co_3O_4 was revealed. The d_{hkl} and relative intensities corresponding to different planes were found and tabulated. Average crystallite size was determined from XRD data using Scherrer equation. Due to the anisotropy of the crystal, strain determination cannot be done by the method of Hall Williamson analysis considering Uniform Deformation Model. DC electrical conductivity showed a gradual rising trend within the selected temperature range of 303 K to 423 K. Using Arrhenius plot, activation energy of synthesised cobalt oxide was calculated as 0.51 eV. For future investigation and extension of present work, certain suggestions are being made. Calcination temperature can be varied and its effect on average crystallite size can be determined. Studies can be done by varying the pH of the sample. Optical, magnetic structural properties of the material could be investigated in detail. Strain determination can be done through Warren-Averbach or Rietweld analysis methods. Comparison of nanocrystalline material with that of its bulk can be done. The oxide material can be synthesised in other dimensions and look upon their significance. Co_3O_4 nanocubes are significant in terms of information storage, electrode material etc. Nanocomposites can be synthesised out of cobalt oxide and their properties can be studied. Nanocomposites like lithium cobalt oxide are good cathode material.

REFERENCES

1. M. Celeste Gardey merino et al (2015) Procedia Materials Science 9, 230-238
2. Xiang et al (2009) Surface Science 603(4),653-658.
3. Masoud Salavati et al (2014) Comptes Rendus Chimie 17(4),352-358.
4. Noboru Yamazoe et al (2003) Catalysis Surveys from Asia 7(1),63-75.
5. Salah.A Makhlouf et al (2013) Superlattices and Microstructures 64,107-117
6. Toshiro Maruyama et al (1996) Journal of the Electrochemical Society 143(4),1383.
7. Arvind Verma etal (2016) Chemical reviews 116(23),14493-14586.
8. Fa-tang Li et al (2015) Nanoscale 7(42), 17590-17610.

9. J. S. Zhang, Q. J. Guo, Y. Z. Liu and Y. Cheng, Ind. Eng. Chem. Res., 2012,51, 12773
10. 10. B D Culitys, in Elements of X-ray Diffraction, II Edition, Addison-Wesley Publishing Company, Inc., Massachusetts (1978)
11. G.K. Williamson, W.H. Hall, Acta Metall. Mater. 1 (1953) 22.
12. A.K.Zak,W.H.A.Majid,M.E.Abrishami,R.Yousefi, SolidStateSci.13(2011) 251–256
13. E.J. Mittemeijer,U.Welzel,Z.Kristallogr.223(2008)552–560.
14. G.K. Williamson,W.H.Hall,ActaMetall.Mater.1(1953)22.
15. G. Madhu,V.C.Bose,K.Maniammal,A.S.A.Raj,V.Biju,PhysicaB421(2013) 87–91
16. V. Biju,N.Sugathan,V.Vrinda,S.L.Salini,J.Mater.Sci.43(2008)1175–1179.
17. I. Bakonyi, E. Toth-Kadar, J. Toth, T. Tarnoczi and A. Cziraki, in: Processing and Properties of Nanocrystalline Materials, eds. C. Suryanarayana et al. (TMS, Warrendale, PA, 1996) p. 465.
18. J.T. Lee, J.H. Hwang, J.J. Mashek, T.O. Mason, A.E. Miller and R.W. Siegel, J. Mater. Res. 10(1995) 2295
19. R.H. Yu, X.X. Zhang, J. Tejada, M. Knobel, P. Tiberto and P. Allia, J. Phys. D 28 (1995) 1770